International Journal of Heat and Mass Transfer 182 (2022) 121917

Contents lists available at ScienceDirect

International Journal of Heat and Mass Transfer

journal homepage: www.elsevier.com/locate/hmt

# Phonon heat transport in two-dimensional phagraphene-graphene superlattice

O. Farzadian [a,*], F. Yousefi [b], C. Spitas [a], K.V. Kostas [a]

[a] Mechanical and Aerospace Engineering, School of Engineering and Digital Sciences, Nazarbayev University, Nur-Sultan 010000, Kazakhstan
[b] Department of Physics, University of Zanjan, Zanjan, 45195-313, Iran

ARTICLE INFO

*Article history:*
Received 3 May 2021
Revised 9 August 2021
Accepted 29 August 2021
Available online 10 September 2021

*Keywords:*
Phagraphene
superlattices
heat transport
thermal conductivity
kapitza resistance
molecular dynamics

ABSTRACT

In this study, we perform non-equilibrium molecular dynamics simulations to investigate phonon heat transport in a two-dimensional superlattice with equal-sized domains of graphene and phagraphene. Effects on conductivity are examined in relation to modifications of domain sizes, the length of employed nanoribbons and temperature differences between the thermal baths used with the superlattices. We have determined that effective thermal conductivity reaches a minimum value of 155 W/mK for ribbons with a superlattice period of 12.85 nm. This minimum thermal conductivity of graphene-phagraphene superlattices at infinite length is approximately 5%, of pure graphene thermal conductivity, and ≈ 50% of phagraphene thermal conductivity. Minimum thermal conductivity occurs at the transition from coherent to incoherent phonon transport, where the superlattice period is comparable to the phonon coherence length.



## 1. Introduction

Phagraphene (PG) is a relatively novel two-dimensional (2D) graphene (G) allotrope comprising penta- hexa- and hepta-carbon rings. Phagraphene was proposed as a defective graphene in 2015 based on a systematic evolutionary structure searching reported in [1]. The discovery of pharaphene has brought a new scientific opportunity to investigate and consider the applications of such kinds of carbon-based 2D structures. Pereira et al showed that thermal conductivity of phagraphene is one order of magnitude smaller than for pristine graphene [2]. Furthermore, and according to their results, a significant reduction in phonon group velocities is also recorded for phagraphene in comparison to graphene.

Over the past few decades, controlling nanoscale heat transport by considering different two 2D structures with atomic-scale impurities, interfaces and defects has been investigated [3–7]. Study of heat transport in superlattices is one of the most interesting research areas since superlattices offer some unique opportunities in phonon thermal transport study [8,9] and its applications in design of novel thermal management devices; see [10]. A superlattice is a periodic or quasi-periodic combination of different materials, which can be described by the superlattice period $l_p$; see Fig. 1. Superlattices may exhibit emergent properties absent to any of their components. The existence of a thermal conductivity minimum is one of the significant features studied when considering thermal transport in superlattices. This has been presented by many researchers in superlattices of varying compositions; see for example [8,9,11–13]. Minimal thermal conductivity is desirable for thermoelectric materials and thermal insulation. The exhibited behavior can be attributed to the competition between coherent (wave-like) and incoherent (particle-like) phonon thermal transport modes in superlattices. Incoherent transport is dominant when superlattice periods $l_p$ exceed in length the phonon mean free path, while coherent behavior is exhibited with period values below the phonon mean free path. In other words, coherent phonons are subject to wave interference whereas incoherent phonons are subject to diffuse scattering. The type and existence of many inter-media interfaces in superlattices affect phonon scattering which controls heat transmission at the nanoscale level; see [14,15]. Furthermore, there are some attempts to use machine learning techniques to explore thermal conductivity in two-dimensional materials [16,17], which can be generalized to predict thermal conductivity in superlattices.

In this work, we investigate heat transport properties of graphene-phagraphene (G-PG) superlattice nanoribbons with a fixed width and equal-sized domains of graphene and phagraphene, as shown in Fig. 1. Our study is performed via non-equilibrium molecular dynamics simulations with armchair G-GP interfaces only. We analyze conductivity dependence on supercell sizes, length of the nanoribbons and we also consider the effect

* Corresponding author.
*E-mail address:* omid.farzadian@nu.edu.kz (O. Farzadian).

https://doi.org/10.1016/j.ijheatmasstransfer.2021.121917
0017-9310/

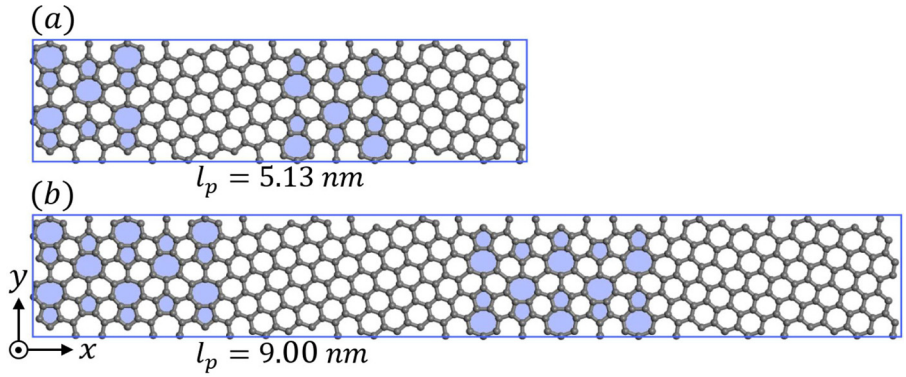


**Fig. 1.** Two G – PG superlattice structures with varying unit cell sizes and periods. Both unit cell have a width of 1.31 nm. Width of the G-PG sheet, are fixed for all cases by eight times replicating of the depicted unit cells in y-direction.

of temperature difference of the employed thermal baths. In connection to our investigation of nanoribbon's length effect on conductivity, an effective phonon mean free path (MFP) is determined whose value is, similarly to conductivity, linked to superlattice period.

The remaining part of this work is structured as follows: Section 2 presents the problem formulation and describes the employed computational approach. Subsequently, in §3, our simulation results are displayed and discussed. This is mainly performed through a series of graphs which visualizes the correlation of the effective thermal conductivity with supercell sizes, the length of employed ribbons and temperature difference. Kapitza resistance at the interface along with phonon density of states (DOS) are used here to illustrate the mechanism for interfacial thermal resistance. Finally, we conclude this work with a brief summary and remarks regarding potential future research directions in §4.

## 2. Problem formulation and computational approach

The Large-scale Atomic/ Molecular Massively Parallel Simulator (LAMMPS)[1] [18] is used for performing all molecular dynamics simulations in our work. Thermal conductivity in nanoribbons is calculated via non-equilibrium molecular dynamics (NEMD) simulations with periodic boundary conditions along both in-plane directions and a free boundary condition in the perpendicular direction. The optimized Tersoff potential by Lindsay and Broido [19] is considered for interactions between carbon atoms and Verlet intergration, with a time-step of 1 fs, is employed in particles trajectory calculations.

We form the employed monolayer superlattice nanoribbons by repeating successively unit cells of graphene and phagraphene of the same size, i.e., equal to the lattice period $l_p$, as depicted in Fig. 1. Although varying length of the ribbons in x-direction are studied, the ribbon width, by eight times replicating of the depicted unit cell in Fig. 1 in y-direction, remains fixed and equal to 10.5 nm. Finally, the thickness of the ribbon corresponds to the thickness of pristine graphene, i.e., 0.34 nm, since this is a monolayer 2D structure.

Proper calculation of thermal conductivity for the G-PG superlattice requires a series of phases that are briefly described here. Initially, energy minimization is performed for positioning atoms in the system. Then, we implement a relaxation phase via an NPT (constant atom number, pressure, and temperature) ensemble with the use of the Nosé-Hoober thermostat and barostat [20]. In this procedure, the structure reaches zero pressure and a temperature of 300 K in 100 ps. In order to achieve zero-stress along the periodic direction (x-axis), zero average stress is considered along the remaining directions. Afterwards, equilibrium is achieved with an NVE (constant atom number, volume, and energy) ensemble for 1 ns to further relax the system at 300 K. Finally, a hot and cold bath, coupled with Nosé-Hoover thermostats and appropriate temperature difference, are set on the two longitudinal ends of the nanoribbon (x-axis). This essentially imposes a temperature gradient and generates heat flow.

Following the abovementioned series of preparatory steps, a 6ns time interval is used for recording our main results. It is also worth mentioning here that the NVE ensemble is applied to the region between the baths. Heat flux is generated by continuous exchange of energy between the hot atoms in the cold region and cold ones in the hot region. Fig. 2 depicts the accumulated energy extracted from the hot bath or equivalently, the energy added to the cold one. The depicted graphs corresponds to a sample length of $L = 40$ nm under a $\Delta T = 40$K thermal-baths temperature difference.

As can easily seen from the same figure, conservation of energy is satisfied as the energy extracted from the hot bath equals the amount added to the cold one. Heat flux along the x-direction, $J_x$, can be computed with the aid of the energy line slope, as follows:

$$J_x = \frac{1}{A}\frac{dE}{dt}, \tag{1}$$

where E denotes the accumulated energy exchanged with the thermostats, t is the simulation time and $A$ corresponds to the cross-sectional area $(0.34 \times 10.5)\,\text{nm}^2$ of our ribbon. For the case depicted in Fig. 2, i.e., $1.58\ \frac{\text{keV}}{\text{ns}}$, the heat flux corresponds to $J_x = 443\ \frac{\text{eV}}{\text{ns}\cdot\text{nm}^2}$.

Once steady state conditions have been reached, we may obtain thermal conductivity for a sample of size L directly from Fourier law with the aid of heat flux and temperature gradient:

$$\kappa_L = \frac{\langle J_x \rangle}{\langle \nabla_x T \rangle}, \tag{2}$$

where $\langle \cdot \rangle$ indicates time averages and $\nabla_x T$ is the temperature gradient in the direction of heat flow. For the evaluation of the temperature gradient, in the stationary regime, we divide the simulated region into several slabs uniformly distributed along the direction of the heat flux. According to the equipartition theorem, the temperature $T_i$ of the $i^{th}$ slab can be calculated from the average kinetic energy of the particles within the slab, as:

$$T_i = \frac{2}{3N_i k_B}\sum_{j}^{N_i}\frac{p_j^2}{2m}, \tag{3}$$

[1] https://lammps.sandia.gov/

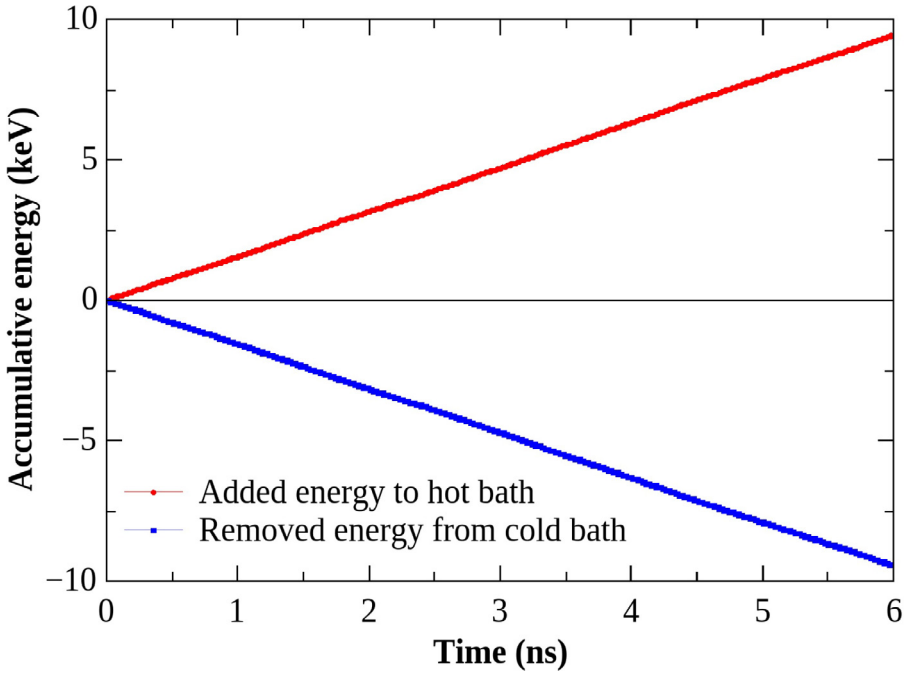


**Fig. 2.** Accumulated energies with time for a sample length of 40 nm at a temperature difference $\Delta T = 40$ K.

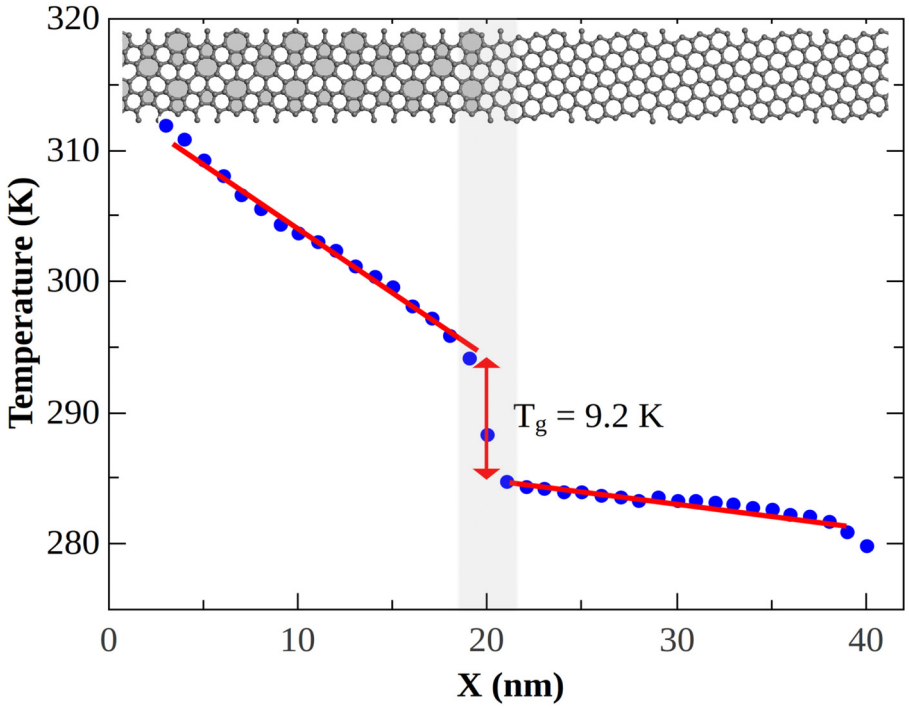


**Fig. 3.** Temperature profile along the longitudinal-direction with $L = 40$nm and $\Delta T = 40$ k.

where $N_i$ is the number of atoms in the $i^{th}$ slab, $k_B$ denotes Boltzmann's constant, and $m$, $p_j$ are the atomic mass and corresponding momentum, respectively. We obviously average temperature values over the last 6 ns of the simulation, i.e., after steady state has been established. Fig. 3 illustrates the temperature profile corresponding to a sample length of $L = 40$ nm with bath-temperature difference of $\Delta T = 40$K (average temperature of baths $T = 300$ K). It worth mentioning that the obtained temperature profile is not for superlattice with repetition of supercells. As depicted in top part of Fig. 3, we consider right side of the sheet are graphene and other side is phagraphene. The red solid line, included in the same figure, corresponds to a linear trend that closely matches the temperature behavior away from the thermal baths. Temperature change, as can be also seen by our numerical results (blue circles) exhibits a nonlinear behavior near the baths due to the strong phonon scattering.

The depicted temperature jump, with an approximate value of 9.2K, at the interface indicates the existence of interface resistance against scattering of vibrational carriers at the corresponding area. We can plug in this value in the Kapitza resistance equation to calculate it. Specifically, the interfacial thermal resistance or Kapitza resistance, which was introduced by P. L. Kapitza [21], can be com-

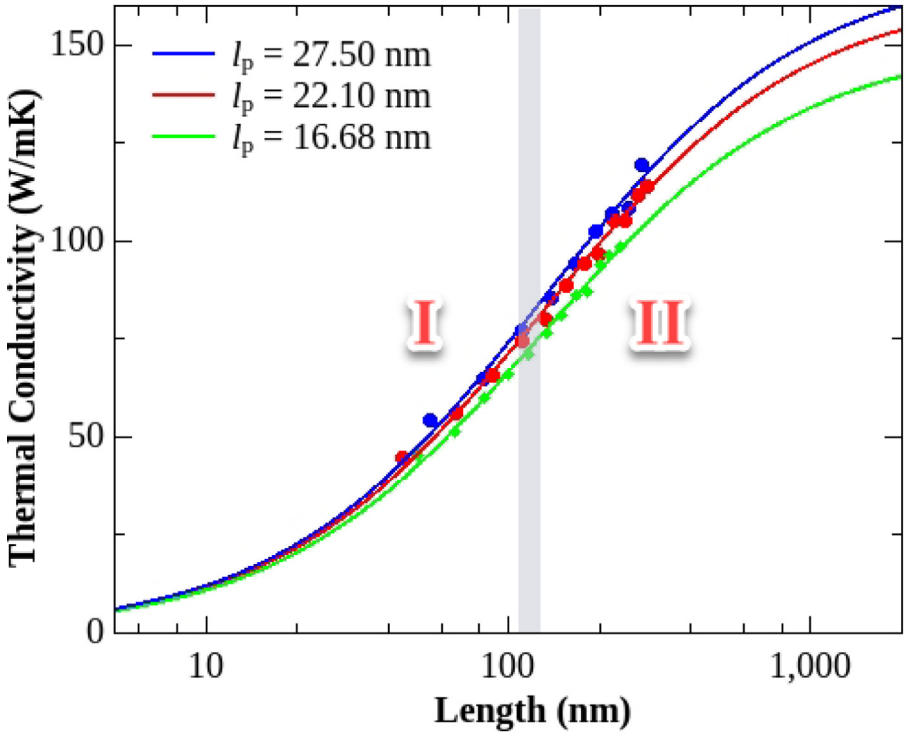


**Fig. 4.** Thermal conductivity dependency on ribbon lengths for three superlattice periods ($l_p$). Data points are extracted from NEMD simulations and solid lines correspond to least-squares fits of Eq. 5 to the corresponding data set. The results, for all system sizes, are calculated based on 10 different simulations, but, for the sake of clarity, error bars are omitted.

puted as follows:

$$R_K = \frac{T_g}{J} \tag{4}$$

where $T_g$ is the temperature gap at the interface ($\approx 9.2$ K) as shown in Fig. 3 and $J$ is the heat flux calculated by Eq. 1. Therefore, Kapitza resistance for this G-PG interface is equal to $12.96 \times 10^{-11}$ $\frac{m^2K}{W}$.

## 3. Results and discussion

Thermal conductivity of a sample with finite length $L$, under the conditions in our numerical setup is expected to follow the following relationship (see [22]):

$$\frac{1}{\kappa_L} = \frac{1}{\kappa_\infty}\left(1 + \frac{\Lambda_{\text{eff}}}{L}\right), \tag{5}$$

where $\kappa_\infty$ is the intrinsic (length-independent) thermal conductivity of the material and $\Lambda_{\text{eff}}$ denotes the effective phonon mean free path. Within this description, the effective MFP corresponds to the length at which $\kappa_L$ equals to 50% of $\kappa_\infty$, i.e, substituting $\Lambda_{\text{eff}} = L$ in Eq. 5 yields $\kappa_L = \frac{1}{2}\kappa_\infty$). For each period of the superlattice, this thermal conductivity is the same as its effective thermal conductivity. Fig. 4 depicts the least-squares fitted relationship described in Eq. 5 (solid lines) to numerical results obtained from Eq. 1 for three different lattice periods. Data points included in Fig. 4 have been obtained by averaging over 10 realizations, with different initial atomic velocities, to account for the computational uncertainties. It is also worth mentioning here that we calculated thermal conductivities for a wide range of periods, $5.13\,\text{nm} \leq l_p \leq 27.50\,\text{nm}$, however only three are included for reasons of clarity. We observe an increase in conductivity with ribbon length for all cases, as expected by Eq. 5. As can be deduced from Fig. 4, thermal conductivity, $\kappa$, depends also on the superlattice period $l_p$ and therefore we may describe it as a function of ribbon length and superlattice period, i.e., $\kappa_L = \kappa(L, l_p)$. Using now these fitted curves and Eq. 5 we can estimate both the intrinsic thermal conductivity $\kappa_\infty$ and the effective phonon MFP, $\Lambda_{\text{eff}}$, for each superlattice period $l_p$. As indicated in Fig. 4, we can distinguish two heat transport regimes that affect the ribbon-length/conductivity relationship. We firstly identify the ballistic regime (region I in Fig. 4) that extends up to lengths of approximately 130mm and in which $\kappa \propto L$. In this region, the phonon MFP is larger than the system length and therefore phonons may travel at distances that exceed the coherence length. For lengths greater than 160 nm (region II in Fig. 4), we enter the diffusive regime in which $\kappa$ shows a weak dependence on system length and the phonon MFP is shorter than the system length. Finally, as expected, between these two regions there is a ballistic-diffusive transition regime, depicted with a gray overlay in Fig 4. Within this transient phase, the phonon MFP and system length are of the same size and conductivity's, $\kappa$, dependence on $L$ starts to decrease.

As a next step, we explore the effect of superlattice period $l_p$ on the estimated intrinsic thermal conductivity $\kappa_\infty$ of the G-PG nanoribbons and the effective phonon mean free path $\Lambda_{\text{eff}}$. Fig. 5 presents our NEMD results for an average temperature between the two baths equal to 300 K. It is quite easy to see from Fig. 5(a) that the overall superlattice thermal conductivity is less than the thermal conductivity of either graphene or phagraphene; see also [2,23]. Specifically, thermal conductivity of the superlattice is remarkably reduced, by $\approx 5\%$, when compared to thermal conductivity of pristine graphene, and $\approx 50\%$ when compared to thermal conductivity of phagraphene. We should also note here that these results are in agreement with previous studies regarding the effect of lattice period on thermal conductivity of superlattices; see [8,9]. Moreover, a distinct feature in both graphs (Fig. 5(a) and 5(b)) is the existence of a minimum value (for ther-

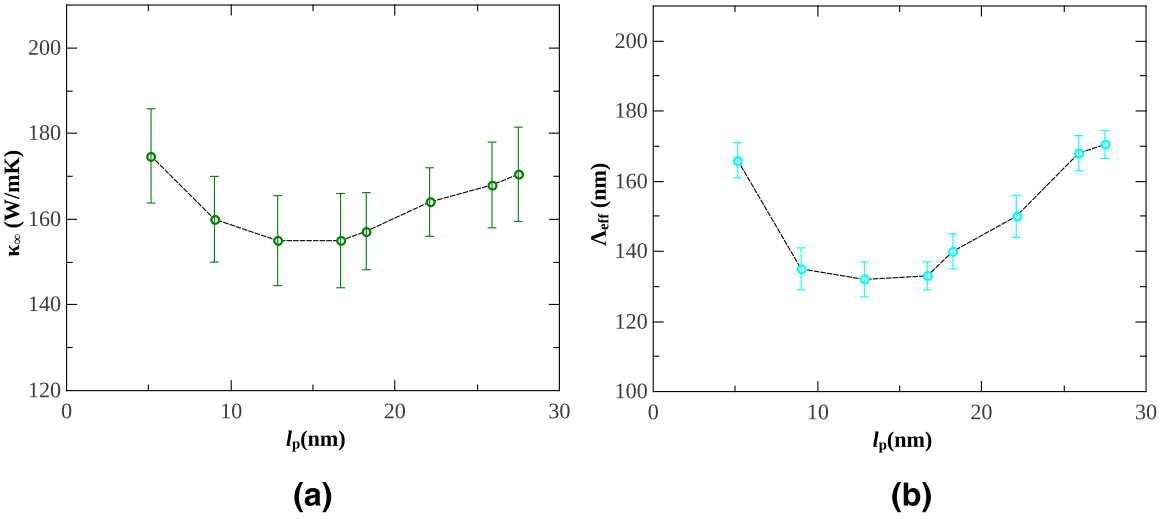


**Fig. 5.** (a) Intrinsic thermal conductivity and (b) effective phonon mean free path as a function of superlattice period. The error bars for all system sizes are calculated based on 10 different simulation runs.

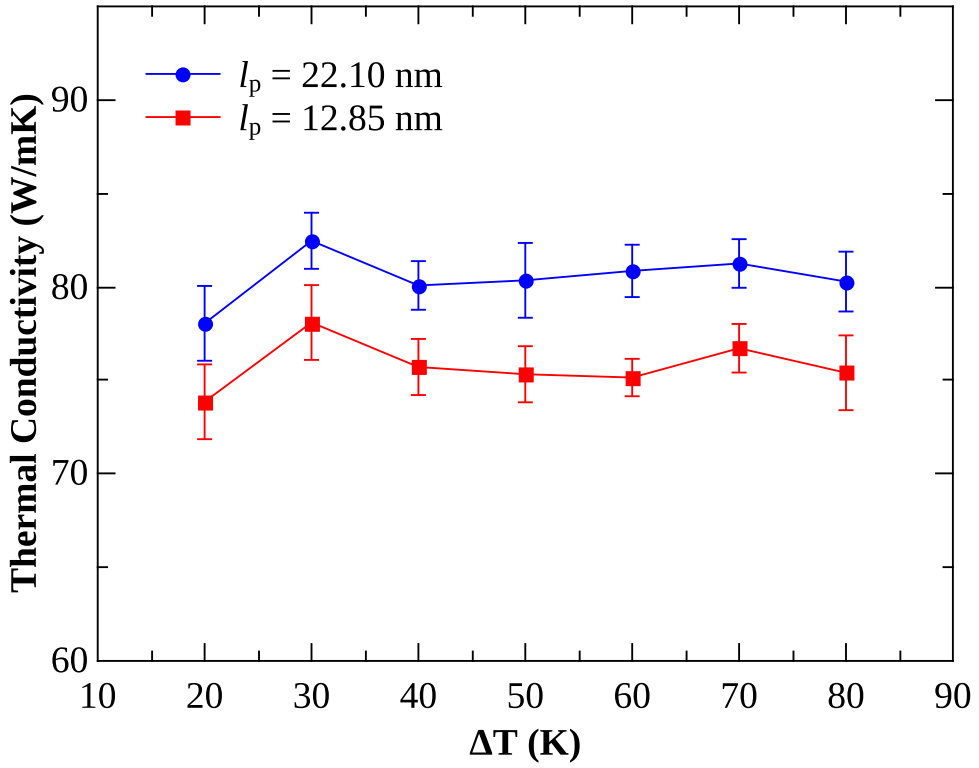


**Fig. 6.** Thermal conductivity as function of temperature differences, $\Delta T$, between thermal baths for two superlattices with periods $l_p = 12.85$ nm and $l_p = 22.10$ nm. Error bars are calculated from 10 different simulation runs.

mal conductivity and effective MFP, respectively) for a superlattice period equal to 12.85 nm. The existence of a single minimum in the function of thermal conductivity, as illustrated in our simulations, is in excellent agreement with what has been reported for various configurations and types of superlattices; see [8,9,24–26]. This phenomenon occurs at the transition from coherent to incoherent phonon transport and it is further explained in [8]. Obviously, the exact value of this minimum thermal conductivity is subject to variations due to numerical inaccuracies as well as the employed the dimensions of the superlattice ribbon employed in each study.

To further clarify the observed trends in thermal conductivity of superlattices, an additional discussion on the effective MFP and phonon coherence length is due. The effective phonon mean free path indicates the average phonon travel distance before scattering, while the coherence length demarcates the length at which the wave-like behavior of phonons becomes important relative to particle-like behavior [27]. When superlattice period is comparable to phonon coherence length, a transition from coherent to incoherent phonon transport occurs. From the data in Fig. 5(b) we estimate phonon coherence length in the order of 12.85 nm which is 10 times smaller than $\Lambda_{\text{eff}}$ value. This essentially means that phonons reach distances much larger than the coherence length, which is also in agreement with the increasing trend in thermal conductivity shown in Fig. 4.

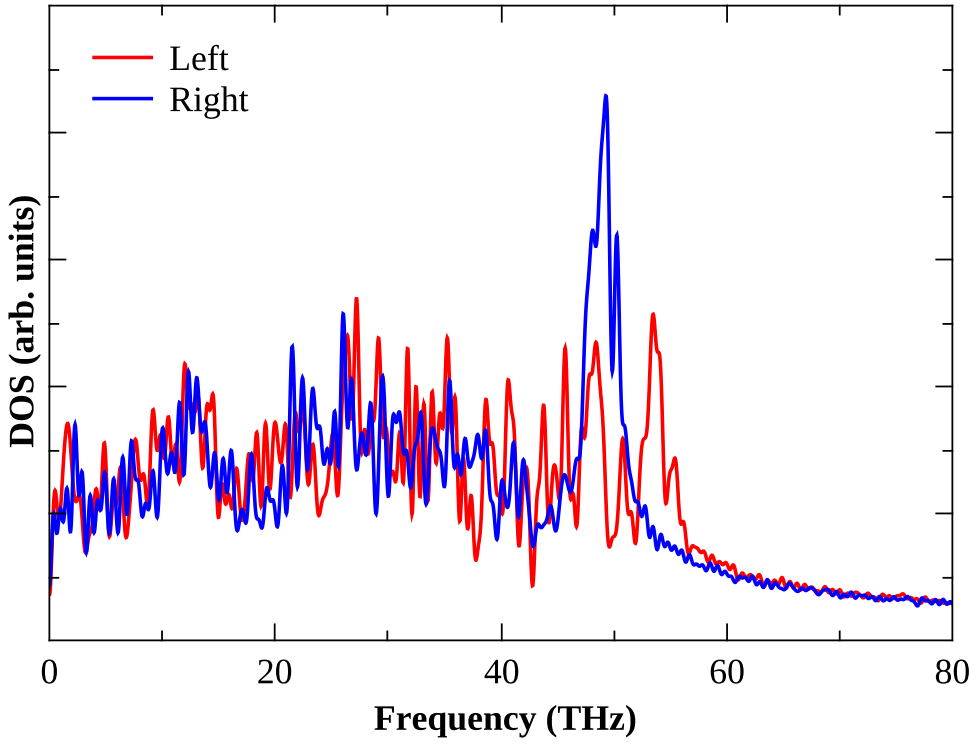


**Fig. 7.** Phonon power spectral density of states on two sides of the G-PG interface at $T = 300\,\mathrm{K}$ and $\Delta T = 40\,\mathrm{K}$.

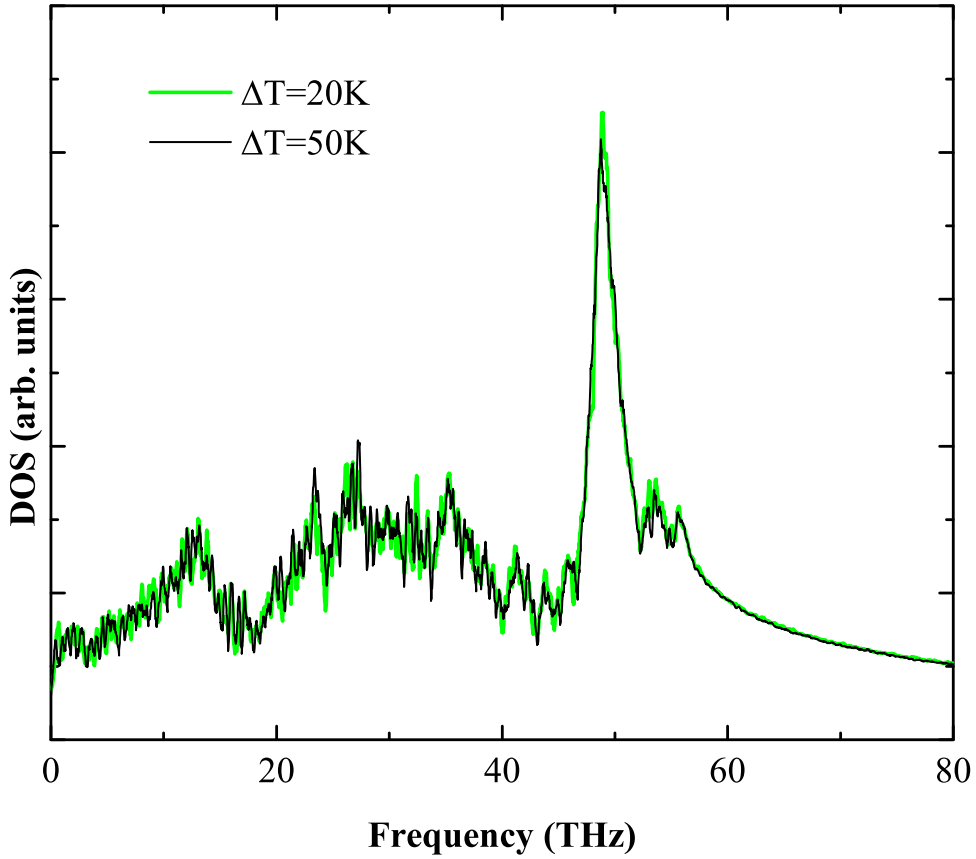


**Fig. 8.** Phonon power spectral density of states for $l_p = 22.10\,\mathrm{nm}$ at $T = 300\,\mathrm{K}$ and $\Delta T = 20\,\mathrm{K}$ and $\Delta T = 50\,\mathrm{K}$.

This series of investigations concludes with the examination of potential effects of the temperature difference, between the employed thermal baths, to thermal conductivity in our structure. Fig. 6 depicts thermal conductivity in terms of this temperature difference, with a fixed average temperature of 300K. Although some small fluctuations are observed, we may consider that thermal conductivity is practically unaffected and we may therefore state that our results are valid for any temperature difference between the two thermal baths.

Finally, to better understand the differences in the interfacial thermal resistance value for the G-PG interface, we calculate phonon spectra of two groups of atoms, corresponding to the graphene and phagrephene sides of the super cell. The density of states (DOS) of phonons on each side is obtained via Fourier transformation of the velocity autocorrelation function $\langle\cdot\rangle$ using the following equation:

$$DOS(\omega) = \frac{m}{k_B T}\int_0^\infty e^{-i\omega t}\langle \boldsymbol{v}(0)\bullet\boldsymbol{v}(t)\rangle dt, \tag{6}$$

where brackets denote averaging over time, and $\omega, m$ and $\boldsymbol{v}$ are the phonon angular frequency, atomic mass and velocity, respectively. $DOS(\omega)$ captures phonon scattering when at the G-PG interface. As shown in Fig. 7, there is a strong mismatch between the left and right spectra. This asymmetry of phonon spectra explains the interfacial thermal resistance and the asymmetrical phonon scattering through the interface. Also, in order to understand the behavior of the calculated thermal conductivity (Fig. 6) with temperature differences, we determined the spectral density of states for different temperature gradients. As illustrated in Fig. 8, there is a rather small deviation between tow spectra for $\Delta T = 20$ K and $\Delta T = 50$ K. Therefore, the effect of temperature differences on thermal conductivity is small, as is also indicated in Fig. 6

## 4. Conclusions

In this study, non-equilibrium molecular dynamics simulations were used in investigating the dependence of thermal conductivity on the total length, period and temperature difference between thermal baths for the Graphene-Phagraphene superlattice. Our results indicate that the minimum thermal conductivity and effective phonon mean free path, at room temperature, are approximately 155 W/mK and 130 nm, respectively. The occurrence of this minimum value at a specific period can be explained if we consider the competition between two factors: conductivity value reduction with decreasing periods and the change in phonon behavior below a certain threshold. Specifically, by decreasing the period length, thermal conductivity is decreased due to the increase in the number of interfaces (thermal resistors), but when the period goes below the identified point, coherent behavior becomes dominant and interface resistant diminishes. Based on our simulation results, thermal conductivity of 2D G-PG superlattices at infinite length is reduced by approximately 5%, compared with the thermal conductivity of graphene, and up to $\approx$ 50% when compared with the thermal conductivity of phagraphene. Also, Kapitza resistance value at G-PG interface were also computed and found to be equal to $12.96\times10^{-11}\ \frac{\mathrm{m^2K}}{\mathrm{W}}$. The results of this study, can be potentially useful in thermal design of novel thermal management devices whit minimum thermal conductivity.

## Credit Author Statment

All persons who meet authorship criteria are listed as authors, and all authors certify that they have participated sufficiently in the work to take public responsibility for the content, including participation in the concept, design, analysis, writing, or revision of the manuscript. Furthermore, each author certifies that this material or similar material has not been and will not be submitted to or published in any other publication before its appearance in the International Journal of Heat and Mass Transfer.

## Declaration of Competing Interest

The authors declared that there is no conflict of interest. The authors declare that they have no known competing financial interests or personal relationships that could have appeared to influence the work reported in this paper.

## Acknowledgments

This work has been funded by the Nazarbayev University Collaborative Research Project (CRP): “Development of smart passive-active multiscale composite structure for earth Remote Sensing Satellites (RSS) of ultrahigh resolution (ULTRASAT)”, Grant Award Nr. 091019CRP2115.

## References

[1] Z. Wang, X.-F. Zhou, X. Zhang, Q. Zhu, H. Dong, M. Zhao, A.R. Oganov, Phagraphene: a low-energy graphene allotrope composed of 5-6-7 carbon rings with distorted dirac cones, Nano Lett. 15 (2015) 6182–6186, doi:10.1021/acs.nanolett.5b02512.
[2] L.F.C. Pereira, B. Mortazavi, M. Makaremi, T. Rabczuk, Anisotropic thermal conductivity and mechanical properties of phagraphene: a molecular dynamics study, RSC Adv. 6 (2016) 57773–57779, doi:10.1039/C6RA05082D.
[3] S. Hu, Z. Zhang, P. Jiang, J. Chen, S. Volz, M. Nomura, B. Li, Randomness-induced phonon localization in graphene heat conduction, J. Phys. Chem. Lett. 9 (2018) 3959–3968, doi:10.1021/acs.jpclett.8b01653.
[4] X. Gu, Y. Wei, X. Yin, B. Li, R. Yang, Colloquium: phononic thermal properties of two-dimensional materials, Rev. Mod. Phys. 90 (2018), doi:10.1103/RevModPhys.90.041002. 041002–30
[5] F. Yousefi, F. Khoeini, Impact of topological line defects on wall roughness and thermal conductivity of carbon nanotubes: a molecular dynamics study, AIP Adv 9 (2019), doi:10.1063/1.5089005. 025024–6
[6] O. Farzadian, A. Razeghiyadaki, C. Spitas, K.V. Kostas, Phonon thermal rectification in hybrid graphene-c3n: a molecular dynamics simulation, Nanotechnology 31 (2020), doi:10.1088/1361-6528/abb04b. 485401–6
[7] O. Farzadian, C. Spitas, K.V. Kostas, Graphene-carbon nitride interface-geometry effects on thermal rectification: a molecular dynamics simulation, Nanotechnology 32 (2021), doi:10.1088/1361-6528/abe786. 215403–6
[8] I.M. Felix, L.F.C. Pereira, Thermal conductivity of graphene-hBN superlattice ribbons, Sci. Rep. 8 (2018), doi:10.1038/s41598-018-20997-8. 2737–10
[9] F.I.M. Felix, L.F.C. Pereira, Suppression of coherent thermal transport in quasiperiodic graphene-hBN superlattice ribbons, Carbon N Y 160 (2020) 335–341, doi:10.1016/j.carbon.2019.12.090.
[10] P. Vaqueiro, A.V. Powell, Recent developments in nanostructured materials for high-performance thermoelectrics, J. Mater. Chem. 20 (2010) 9577–9584, doi:10.1039/C0JM01193B.
[11] L. Razzaghi, F. Khoeini, A. Rajabpour, Maryam khalkhali, thermal transport in two-dimensional c 3 n/c 2 n superlattices: a molecular dynamics approach, Int. J. Heat Mass Transf. 177 (2021), doi:10.1016/j.ijheatmasstransfer.2021.121561. 121561–5
[12] Y. Chen, D. Li, J.R. Lukes, Z. Ni, M. Chen, Superlattice thermal conductivity from molecular dynamics, Phys. Rev. B 72 (2005), doi:10.1103/PhysRevB.72.174302. 174302–6
[13] J.-W. Jiang, J.-S. Wang, B.S. Wang, Minimum thermal conductance in graphene and boron nitride superlattice, Appl. Phys. Lett. 99 (2011), doi:10.1063/1.3619832. 043109–3
[14] M.N. Luckyanova, et al., Coherent phonon heat conduction in superlattices, Science 338 (2012) 936–939, doi:10.1126/science.1225549.
[15] J. Ravichandran, et al., Crossover from incoherent to coherent phonon scattering in epitaxial oxide superlattices, Nat. Mater. 13 (2014) 168–172, doi:10.1038/nmat3826.
[16] B. Mortazavi, I.S. Novikov, E.V. Podryabinkin, S. Roche, T. Rabczuk, A.V. Shapeev, X. Zhuang, Exploring phononic properties of two-dimensional materials using machine learning interatomic potentials, Appl. Mater. Today 20 (2020), doi:10.1016/j.apmt.2020.100685. 100685–10
[17] B. Mortazavi, E.V. Podryabinkin, I.S. Novikov, S. Roche, T. Rabczuk, X. Zhuang, A.V. Shapeev, Efficient machine-learning based interatomic potentials for exploring thermal conductivity in two-dimensional materials, J. Phys. Mater. 3 (2020), doi:10.1088/2515-7639/ab7cbb. 02LT02-10
[18] S. Plimpton, Fast parallel algorithms for short-range molecular dynamics, J. Comput. Phys. 117 (1995) 1–19, doi:10.1006/jcph.1995.1039.
[19] L. Lindsay, D.A. Broido, Optimized tersoff and brenner empirical potential parameters for lattice dynamics and phonon thermal transport in carbon nanotubes and graphene, Phys. Rev. B 81 (2010), doi:10.1103/PhysRevB.81.205441. 205441–6

[20] S. Melchionna, G. Ciccotti, B.L. Holian, Hoover npt dynamics for systems varying in shape and size, Mol. Phys. 78 (1993) 533–544, doi:10.1080/00268979300100371.
[21] P.L. Kapitza, Heat transfer and superfluidity of helium II, Phys. Rev. 60 (1941) 354–355, doi:10.1103/PhysRev.60.354.
[22] P.K. Schelling, S.R. Phillpot, P. Keblinski, Comparison of atomic-level simulation methods for computing thermal conductivity, Phys. Rev. B 65 (2002), doi:10.1103/PhysRevB.65.144306. 144306–12
[23] B. Mortazavi, T. Rabczuk, Multiscale modeling of heat conduction in graphene laminates, Carbon N Y 85 (2015) 1–7, doi:10.1016/j.carbon.2014.12.046.
[24] L. Zhu, B. Li, Low thermal conductivity in ultrathin carbon nanotube (2, 1), Sci. Rep. 4 (2014) 491–496, doi:10.1038/srep04917.
[25] X.-K. Chen, Z.-X. Xie, W.-X. Zhou, L.-M. Tang, K.Q. Chen, Phonon wave interference in graphene and boron nitride superlattice, App. Phy. Lett. 109 (2016), doi:10.1063/1.4958688. 023101–5
[26] C.d. Silva, F. Saiz, D.A. Romero, C.H. Amon, Coherent phonon transport in short-period twodimensional superlattices of graphene and boron nitride, Phy. Rev. B 93 (2016), doi:10.1103/PhysRevB.93.125427. 125427–10
[27] T. Zhu, E. Ertekin, Phonon transport on two-dimensional graphene/boron nitride superlattices, Phys. Rev. B 90 (2014), doi:10.1103/PhysRevB.90.195209. 195209–9